Thermogravitational separation in porous vertical and horizontal cylindrical annular cells saturated by a binary mixture

Khairi Sioud, Ali Abdennadher, Alain Bergeon, Slim Kaddeche, Marie Catherine Charrier Mojtabi, AbdelKader Mojtabi

Eur. Phys. J. E manuscript No.
(will be inserted by the editor)

Thermogravitational separation in porous vertical and horizontal cylindrical annular cells saturated by a binary mixture

Khairi Sioud[1,2], Ali Abdennadher[2], Alain Bergeon[1], Slim Kaddeche[3], Marie Catherine Charrier-Mojtabi[1], Abdelkader Mojtabi[a,1]

[1]Université de Toulouse, I.M.F.T. UMR CNRS/INP/UPS, 31400 Toulouse, France
[2]Université de Carthage, EPT, LIM (LR 01-ES-13), 2078, La Marsa, Tunisie
[3]Université de Carthage, INSAT, MMA (LR 11-ES-25), 1080, Tunis, Tunisie

Received: date / Accepted: date

Abstract In this paper, analytical and numerical studies of species separation in vertical and horizontal porous, cylindrical annular cells were presented. The binary fluid, saturating the porous medium, is a water-ethanol mixture. The thickness e, of the horizontal and vertical columns is equal to $R_o - R_i$, where R_i and R_o are respectively the internal and the external radii. H is the height of the vertical cell, and the length of the horizontal cell. Constant temperatures, T_{hot} and T_{cold}, were imposed on the inner and outer cylinders. Since an important species separation, in thermo-gravitational column (TGC), is obtained for $e << H$, the same assumption was made for the two configurations. The analytical solution was obtained using the parallel flow approximation for both configurations. The governing equations were solved numerically for 2D and 3D configurations using two different softwares (Comsol Multiphysics and a spectral collocation method with Gauss-Lobatto-Chebyshev points). Velocity, temperature, mass fraction fields and time to reach steady state were compared for the two configurations. The amount of species separated at the top or the bottom of each cell was also compared for each configuration.

Program Summary and Specifications

Program title:
Licensing provisions:
Programming language:
Repository and DOI:
Description of problem:
Method of solution:
Additional comments:

1 Introduction

If a temperature gradient is applied to a binary or multi-component mixture, a mass fraction gradient appears for each species. Thus the expression of the mass flux density vector $\mathbf{J}'_m$ is given by Fick's law with another term proportional to the temperature gradient namely Soret contribution:

$$\mathbf{J}'_m = -\rho' D^* \nabla C - \rho' {D_T}^* \nabla T' \quad (1)$$

Where ρ', D^* are respectively the density of the binary fluid, the mass diffusion coefficient of the denser component and ${D_T}^*$ its thermodiffusion coefficient in the porous medium. C and T' are respectively the mass fraction of the denser component and the temperature. The species separation due to thermodiffusion or Soret effect are very weak. So if we consider the coupling between thermodiffusion and natural convection called thermo-gravitational diffusion, the species separation may increase. Thermo-gravitational diffusion has been widely studied due to its numerous fundamental and industrial applications. A summary of these applications were detailed by Nield and Bejan [1], Vafai [2] and Legros et al. [3]. The Soret effect in liquid mixtures has been reviewed by Khöhler et al. [4]. The first thermogravitational columns (TGC) were filled with bi-

[a]e-mail: mojtabi@imft.fr

nary fluids. Furry, Jones and Onsager, developed the theory of thermodiffusion to interpret the experimental processes of isotope separation [5]. In their study the authors assumed that the density of the binary fluid depends only on the temperature and not on the mass fraction, in gravity forces, this was commonly called the forgotten effect. In 1959, Lorenz and Emery [6] considered vertical columns (TGC) filled with porous packing saturated by a binary fluid in order to increase the thickness of the cell leading to maximum species separation. Research on species separation in vertical thermogravitational columns (TGC) has been performed for a long time. In 2003, Platten et al. [7] studied experimentally the effect of the tilt, relative to the horizontal direction, of a rectangular cell heated only from below. Then several papers were devoted to the horizontal porous configuration saturated by a binary fluid, in order to improve the species separation. Charrier-Mojtabi et al. [8] showed that it was possible to obtain the species separation in a horizontal cell heated from below. The authors studied the influence of the separation ratio, $\psi = -\frac{\beta_C}{\beta_T}\frac{{D_T}^*}{D^*}C_0(1-C_0)$, ($\beta_T$, β_C and C_0 are defined in §2) and the normalized porosity on the stability of the equilibrium solution, theoretically and numerically. Seta et al. [9] studied instabilities in DCMIX1 ternary mixtures when two liquid layers with different concentrations are superimposed. El Hajjar et al. [10] studied the species separation in a porous horizontal cell for negative or positive values of the separation ratio leading to the onset of a unicellular flow. El Hajjar et al. [11] considered a shallow porous cavity filled with a binary fluid. The cavity was heated from below or from above and was inclined with respect to the vertical axis. The authors showed analytically and numerically that the species separation can be increased for an optimal value of the tilt angle of the cavity. Further studies have been carried out for porous horizontal layers saturated by a binary fluid with various boundary conditions. Khouzam et al. [12] used mixed convection in order to study the species separation in a horizontal porous cell. Yacine et al. [13] considered the case of a porous cavity that was subjected to cross heat fluxes. Yasnou et al.[14] studied experimentally the thermodiffusion dynamics in a compound system when a layer of a porous medium is surrounded by free liquids. Mojtabi et al. [15] studied a new configuration of the horizontal porous layer by moving the cavity walls at a constant and opposite velocity. Abahri et al. [16] analyzed, for the first time, the species separation in a horizontal porous annulus. An analytical resolution using a perturbation method till order two and function of the Rayleigh number was presented. The analytical results were corroborated by numerical results obtained with a finite element method (Comsol Mutiphysics). Thermogravitational separation and time to reach the steady state have been studied recently by Seta et al. [17]. Nasrabadi et al. studied, experimentally, the influence of permeability on species separation and time to reach steady state in a thermogravitational column filled with a porous medium [18]. First, there has never been before a comparative study dealing with the species separation in a horizontal and in a vertical porous annular column. In the case of the horizontal column, article [16], only an approximate analytical solution using the perturbation method, developed at order two, was obtained. We performed in the present paper 3D numerical simulations which verified the validity of the 2D results presented in the article [19]. We also checked that the results of the 3D numerical simulations were in good agreement with those of the 2D numerical simulations. The authors examine, analytically and numerically, the species separation in horizontal and vertical porous cylindrical annular cells saturated by a binary water-ethanol mixture. The species separations at steady state were compared as well as the time needed to reach this steady state.

2 Mathematical formulation

The vertical and horizontal porous cylindrical annular cells are presented in fig.1. The binary fluid saturating the porous medium is a water-ethanol mixture (60.88% water). The thickness of the horizontal and the vertical column is: $e = R_o - R_i$, where R_i and R_o are the internal and the external radii respectively. $H = \pi R_i$ is the height of the vertical column, and the length of the horizontal cell. Constant temperatures, T_{hot} and T_{cold} were imposed on the inner and outer cylinders. The fluid flow within the porous medium is assumed to be incompressible and governed by Darcy's law. It is also assumed that viscous dissipation and Dufour effect are neglected since their influence is very weak in the considered liquid mixtures. Also, the Boussinesq approximation is considered for binary fluid properties which are considered as constant except the density of the fluid in the buoyancy contribution which varies linearly with both local temperature and local mass fraction:

$$\rho' = \rho_0(1 - \beta_T(T' - T_0) - \beta_C(C - C_0)) \tag{2}$$

where, ρ_0, β_T, β_C are respectively the density of the binary fluid at the reference state T_0 and C_0, the thermal and solutal expansion coefficients. Under these assumptions, the continuity equation, the Darcy's law, and the conservation equations of energy and chemical species are written in dimensional form as follows:

$$
\begin{aligned}
\nabla \cdot \mathbf{V}' &= \mathbf{0} \\
\mathbf{V}' &= -\frac{K}{\mu}(\nabla \mathbf{P}' - \rho_0[1 - \beta_T(T' - T_0) - \beta_C(C - C_0)]\mathbf{g}) \\
(\rho c)^* \frac{\partial T'}{\partial t'} &+ (\rho c)_f \mathbf{V}' \cdot \nabla T' = \lambda^* \nabla^2 T' \\
\epsilon^* \frac{\partial C}{\partial t'} &+ \mathbf{V}' \cdot \nabla C = D^* \nabla^2 C + {D_T}^* C_0(1 - C_0)\nabla^2 T'
\end{aligned}
\tag{3}
$$

$\mathbf{V}'$ and $\mathbf{P}'$ are respectively the velocity of the flow and the pressure. In these equations λ^*, $(\rho c)^*$ are respectively the effective thermal conductivity and the effective volumetric heat capacity of the porous medium-mixture system and $(\rho c)_f$ is the volumetric heat capacity of the mixture. ϵ^* is the porosity of the porous medium.

If Ω' represents the union of surfaces S_i' and S_o' which are respectively the inner and the outer surfaces of the cylinders, the boundary conditions associated with system (3) are system (4).

$$
\begin{aligned}
\mathbf{V}'(M \in \Omega') \cdot \mathbf{n} &= 0 \\
T'(M \in S_i') &= T_{hot} \\
T'(M \in S_o') &= T_{cold} \\
\text{For}(M \in S_i' \cup S_o'); (D^* \nabla C + {D_T}^* C_0(1 - C_0)\nabla T') \cdot \mathbf{n} &= 0
\end{aligned}
\tag{4}
$$

The base surfaces are insulated and impermeable in each configuration:

$$
\nabla C \cdot \mathbf{n} = 0; \nabla T' \cdot \mathbf{n} = 0 \tag{5}
$$

The height $H = \pi R_i$ was chosen so that the length of the streamlines would be almost equal in the two configurations. The length of the horizontal cell is chosen equal to H, in order to compare the results obtained for the two configurations.

In order to simplify parametric representation of the physical problem, a dimensionless formulation of system (3) is considered. The reference scales are R_i for the length, $\lambda^*/(R_i(\rho c)_f)$ for the velocity, $((\rho c)^* R_i^2)/\lambda^*$ for time, $(\lambda^* \mu)/(K(\rho c)_f)$ for the pression and δT for the temperature. The dimensionless mathematical formulation of the problem is given by :

$$
\begin{aligned}
\nabla \cdot \mathbf{V} &= \mathbf{0} \\
\mathbf{V} + \nabla \mathbf{P} &= -(Ra_T T + R_S(C - C_0))\mathbf{e_z} \\
\frac{\partial T}{\partial t} &+ \mathbf{V} \cdot \nabla T = \nabla^2 T \\
\epsilon \frac{\partial C}{\partial t} &+ \mathbf{V} \cdot \nabla C = \frac{1}{Le}(\nabla^2 C + A Ra_T \nabla^2 T)
\end{aligned}
\tag{6}
$$

The problem under consideration depends on five non-dimensional parameters: the thermal Rayleigh number $Ra_T = \frac{Kg\beta_T R_i \delta T}{\alpha\nu}$, the equivalent solutal Rayleigh number $R_S = \frac{K\beta_C g R_i}{\alpha\nu}$, the Lewis number $Le = \alpha/D^*$, the modified porosity $\epsilon = \epsilon^*(\rho c)_f/(\rho c)^*$, and a new parameter $A = \frac{D_T^* C_0(1-C_0)\alpha\nu}{D^* K\beta_T g R_i}$ not dependent on δT.

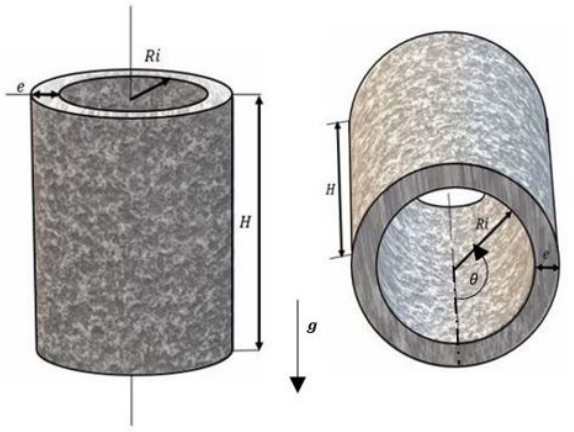

Fig. 1 Annular vertical and horizontal porous cells

Ω represents the union of surfaces S_i where $r = 1$ and S_o where $r = R$, with $R = R_o/R_i$ which are respectively the inner and the outer surfaces.

$$
\begin{aligned}
\mathbf{V}(M \in \Omega) \cdot \mathbf{n} &= 0 \\
T(M \in S_i) &= 1 \\
T(M \in S_o) &= 0 \\
\text{For}(M \in S_i \cup S_o); (\nabla C + A Ra_T \nabla T) \cdot \mathbf{n} &= 0
\end{aligned}
\tag{7}
$$

The dimensionless boundary conditions at base surfaces would be as following:

$$
\nabla C \cdot \mathbf{n} = 0; \nabla T \cdot \mathbf{n} = 0 \tag{8}
$$

3 Analytical resolution

3.1 Vertical porous cell

For the vertical porous cylindrical cell, the following approximations were taken into account in order to simplify the resolution:

$$
\begin{cases}
T = f(r) \\
\mathbf{V} = V(r)\mathbf{e}_z \\
C = mz + h(r)
\end{cases}
\tag{9}
$$

When we take into consideration the boundary conditions (7, 8) for the resolution of the set of equations (6), the temperature is written as:

$$
T = 1 - \frac{\ln(r)}{\ln(R)} \tag{10}
$$

In our case $e << R_i$ and the flow is axisymmetric with respect to $\mathbf{e_z}$ which allow us to assume that the vertical

annular cell can be considered as a cell between two vertical planes heated differentially. Thus the velocity expression of $V(r)$ noted $V_2(r)$ can be written as:

$$V_2 = \frac{Ra_T(R\ln(R) - (\ln(r)+1)(R-1))}{(R-1)\ln(R)} \quad (11)$$

and the associated mass fraction is noted

$$C_2 = m_2 z + h_2(r) \quad (12)$$

where the expressions of m_2 and $h_2(r)$ are given in Appendix A). If the curvature effect is taken into account for the annular cylindrical column, we obtain for the velocity $V(r)$ an expression different from $V_2(r)$ noted $V_3(r)$ given by:

$$V_3 = \frac{Ra_T(2R^2\ln(R) - 2\ln(r)R^2 - R^2 + 2\ln(r) + 1)}{2(R^2-1)\ln(R)} \quad (13)$$

Fig.2 shows a good accuracy between velocities $V_2(r)$ and $V_3(r)$ although their expressions are different.
We also consider that, for the cylindrical cell, the continuous sum of the mass fraction is conserved in the cylindrical cell and the total mass flux through any annular horizontal surface is equal to zero which lead us to the expression of mass fraction C_3:

$$C_3 = m_3 z + h_3(r) \quad (14)$$

where the expressions for m_3 and $h_3(r)$ are given in Appendix A.

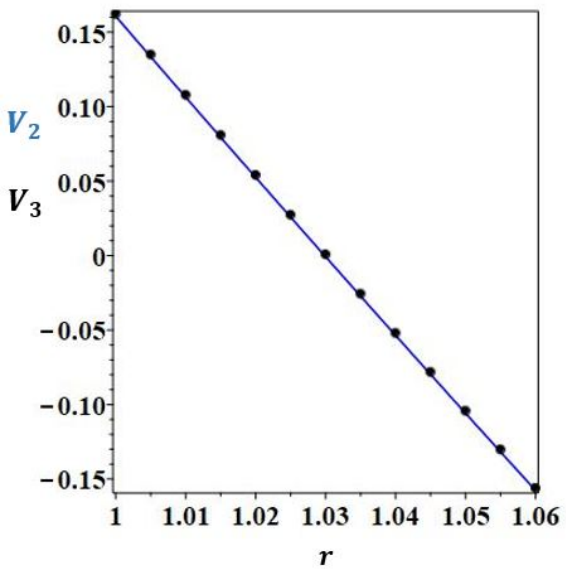

Fig. 2 Comparison between V_2 (blue line) and V_3 (black dots) as a function of r for $R = 1.06$.

On fig.3 are presented, for $r = R_i$ the evolution of the mass fraction according to z obtained for C_2 and C_3. This evolution as a function of z is linear for all values of r with $r \in [R_i, R_o]$. The results obtained with these two approaches are in good agreement.

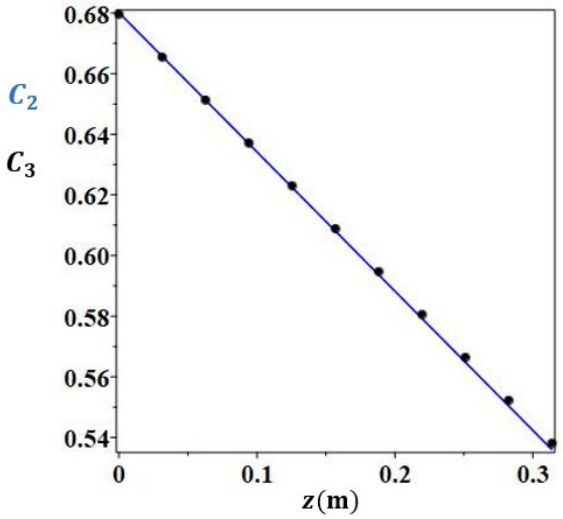

Fig. 3 Comparison between C_2 (blue line) and C_3 (black dots) as a function of z for $R_i = 0.1$ m.

3.2 Horizontal porous cell

In this paragraph, the main analytical results published in the article by Mojtabi et al. [19] are reported in order to compare the importance of species separation in both horizontal and vertical TGC. Natural convection flow between two isothermal cylinders, maintained at constant and different temperatures T_{hot} on the inner cylinder and T_{cold} on the outer cylinder was characterized by a symmetrical flow with respect to the vertical plane containing the axis of the two cylinders. This flow is also invariant in any vertical plane orthogonal to the horizontal axis of the two cylinders. The binary fluid rises along the hot inner cylinder and descends along the cold outer cylinder. This convective regime is all the more stable as $(R_o – R_i)$ and $(T_{hot} – T_{cold})$ are small, Cf.[[20]]. The thermal field obtained in horizontal configuration is purely conductive. It is therefore identical to the one obtained in a vertical configuration, i.e.:

$$T = 1 - \frac{\ln(r)}{\ln(R)} \quad (15)$$

The analytical solution of this problem has been carried out in terms of the stream function, ϕ:

$$\phi = Ra_T sin(\theta) F(r) \quad (16)$$

where $F(r)$ is:

$$F(r) = \frac{R^2(r^2-1)\ln(R) - r^2(R^2-1)\ln(r)}{2r(R^2-1)\ln(R)} \quad (17)$$

Only the species balance equation has been solved numerically from a partial differential equation with the mass fraction, C, as the only unknown:

$$\left(\frac{\partial(r\frac{\partial C}{\partial r})}{\partial r} + \frac{1}{r}\frac{\partial^2 C}{\partial \theta^2}\right) = Le\left(\frac{\partial \phi}{\partial r}\frac{\partial C}{\partial \theta} - \frac{\partial \phi}{\partial \theta}\frac{\partial C}{\partial r}\right) \quad (18)$$

4 Results and discussion

For a binary fluid with a positive thermodiffusion coefficient, $D_T > 0$, the lightest component migrates to the top of the annular duct and the heaviest to the bottom of the cell (As seen in Fig. 8 below): the steady state is stable. However, for negative D_T, it is the opposite situation: the steady state may be instable. This situation for $D_T < 0$, has not been the subject of a stability analysis.

4.1 Comparison between analytical and numerical results

To illustrate the analytical and 2D and 3D numerical results obtained in this study, the authors only considered the experimental values of the thermophysics parametersthe water-ethanol solution (60.88% water - 39.12% ethanol) studied by Platten et al. [7]. The values of the thermophysical properties of this binary solution for an average temperature $T = 22.5°\mathrm{C}$ are detailed in Table.1. Table.2 shows the values of the coefficients of thermodiffusion, D_T^* and mass diffusion, D^* of the water-ethanol binary solution saturating the porous medium are detailed in Table 2. The two values of the permeability K_1 and K_2 of the porous medium and its porosity ϵ^* are also reported.

Table 1 Properties of a water (60.88 wt%) - ethanol (39.12 wt%) mixture at a mean temperature of $22.5°C$.

$D[\mathrm{m^2 s^{-1}}]$	$D_T[\mathrm{m^2(sK)^{-1}}]$	β_C	$\beta_T[\mathrm{K^{-1}}]$
4.32×10^{-10}	1.37×10^{-12}	-0.212	7.86×10^{-4}
$\alpha[\mathrm{m^2 s^{-1}}]$	$\rho_0[\mathrm{kg\ m^{-3}}]$	$\nu[\mathrm{m^2 s^{-1}}]$	
2.23×10^{-7}	935.17	2.716×10^{-6}	

Table 2 Properties of the porous medium at a mean temperature of $22.5°C$.

$D^*[\mathrm{m^2 s^{-1}}]$	$D_T{}^*[\mathrm{m^2(sK)^{-1}}]$	ϵ^*	$K_1[\mathrm{m^2}]$	$K_2[\mathrm{m^2}]$
1.878×10^{-10}	5.96×10^{-13}	0.47	6.58×10^{-10}	2.5×10^{-11}

The values of dimensionless numbers: thermal Rayleigh number Ra_T, radius ratio R, Lewis number Le, solutal Rayleigh number R_S and A used in this study, for a temperature difference of 10°C, are detailed in Table 3.

For both configurations, temperature T is the same function of r. Fig.4 shows the good agreement between the numerical (points) and analytical (solid line) results. The hypothesis leading to $\mathbf{V} = V(r)\mathbf{e}_z$ is perfectly verified in almost all of the central part of the vertical column as indicated in fig.5.

Table 3 Dimensionless parameters for $\delta T = 10°\mathrm{C}$, for $K_2 = 2.5 \times 10^{-11}\ \mathrm{m^2}$.

R	Ra_T	R_S	A	Le
1.06	0.3182	-8.5844	0.0237	1187.4
1.03	0.6365	-17.169	0.0118	1187.4

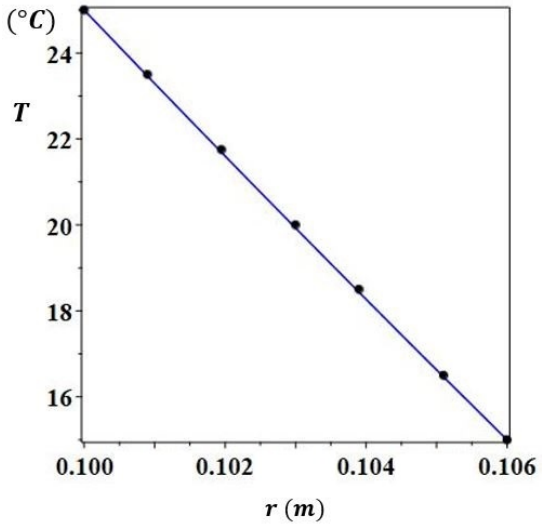

Fig. 4 Numerical (dots) and analytical (continuous line) dimensional temperature T as a function of r.

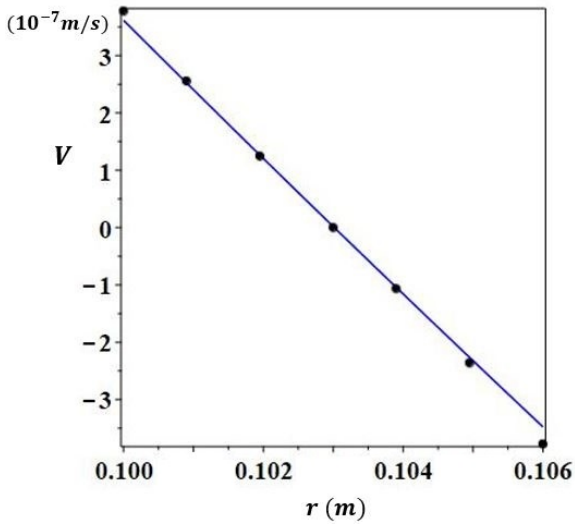

Fig. 5 Numerical(dots) and analytical (line) values of dimensional velocity V in vertical cell as a function of r for $z = H/2$.

However, for the horizontal cells, both radial and angular velocities are not equal to zero. The analytical results obtained for low values of R and moderate values

of Ra_T show that $\mathbf{V}_r \ll \mathbf{V}_\theta$. The tangential velocity $\mathbf{V}_\theta$ given in fig.6 reaches the maximum at $\theta = \pi/2$, when $\mathbf{V}_r$ is equal to 0. Near the values, $\theta = 0, \pi$, $\mathbf{V}_r$ tends to its maximum.

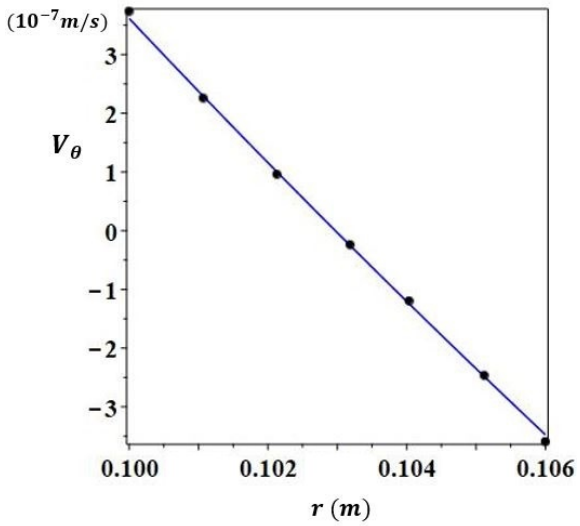

Fig. 6 Numerical(dots) and analytical (line) values of dimensional angular velocity V_θ in horizontal cell as a function of r for $\theta = \pi/2$.

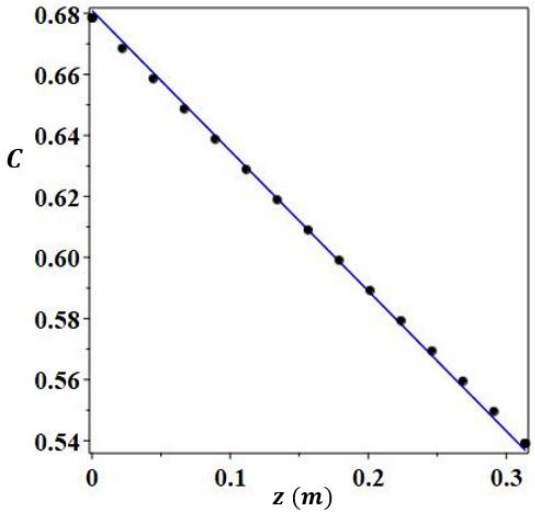

Fig. 7 Numerical (dots) and analytical values of mass fraction in vertical cell as a function of z for $r = (R_i + R_o)/2$, $K_2 = 2.5 \times 10^{-11}$ m^2 and $\delta T = 10°$C.

4.2 Species separation and time to reach the steady state

The system of equations (3) with the boundary conditions (4) and (5), was solved numerically using two different softwares: Comsol Multiphysics with finite elements in 2D and 3D (fig.8) and code written on MATLAB based on a method of spectral collocation, using Gauss Lobatto Chebyshev points. The flow in the vertical porous cell has a vertical symmetry axis $\mathbf{e_z}$. The flow in the horizontal porous annular cell is invariant under translation in any vertical plane perpendicular to the axis of the cell. The study was conducted with a porosity, ϵ^* and two permeabilities, K_1 and K_2. The binary fluid is a water (60.88 wt%)- ethanol (39.12 wt%) solution studied by Platten et al. [7]. The values of the thermophysical properties of this binary solution are mentionned in Table 1 and Table 2. The imposed temperature difference δT and the permeability K in both vertical and horizontal cells were investigated. The analytical result of mass fraction at steady state is found numerically, fig.7, without resorting to the simplifying assumptions used in paragraph 3.1.
Species separation S is defined by: $S = C_{max}$–C_{min}. In all the calculations, the thickness is supposed to be constant: $e = 6 \times 10^{-3}$ m. The respective influence on the species separation, of the internal radius R_i, of the imposed temperature difference δT and of the permeability K in both vertical and horizontal cells, was presented in Table 4, 5, 6 and 7 where comparison between the two methods results are detailed in Table 4 and Table 5. It appears from these various results that the separation $S = C_{max}$–C_{min}:
1°) increases as the value of R_i increases
2°) increases as δT increases
3°) decreases as K increases
As already mentioned, the species separations in horizontal cells are always slightly greater than in vertical cells (for fixed values of R_i and δT).When K increases, the convective velocity increases and becomes higher than the velocity leading to the optimal separation. However the time to reach the steady state when K decreases, increases.Therefore a good compromise must be found between permeability and time to reach steady state. Furthermore, the influence of the value of the inner cylinder is slightly greater than the influence of the temperature difference, Table 5 and 7. On fig.9 and fig.10, we present the variations of C_{max} and C_{min} as a function of time in order to study the time to reach the steady state. The study shows that the steady state was reached for a time of about 6×10^4 s for the vertical annular cell and about 12×10^4 s for the horizontal porous annular layer. Moreover the steady state was reached in the lower part of the horizontal annular cell two times more quickly than in the upper part (fig.10). However, the steady state is reached simultaneously at the top and at the bottom of the vertical annular cell (fig.9). These results obtained numerically only, fig.9

and fig.10, led us to look for the physical reason why the steady state in the vertical configuration is reached faster than in the horizontal configuration. It emerges from the analysis of figures (5) and (6) that the velocity V of the fluid along the vertical axis $\mathbf{e}_z$ is of the same order of magnitude as the tangential velocity V_θ calculated for $\theta = \pi/2$ where it is maximum. As the time to reach the stationary state depends on the number of cycles performed by the fluid particles, we can deduce that the stationary state will be reached first in the vertical column. Fig.9 shows the presence of a maximum and a minimum, in the vertical annular column, just before the stationary state is reached. This result has also been measured experimentally by Seta et al.[15] in a parallelepipedic vertical column. Indeed, the process of thermogravitational separation continues and stops as soon as the reverse process of pure mass diffusion balances the thermogravitational contribution to lead to the stationary state.

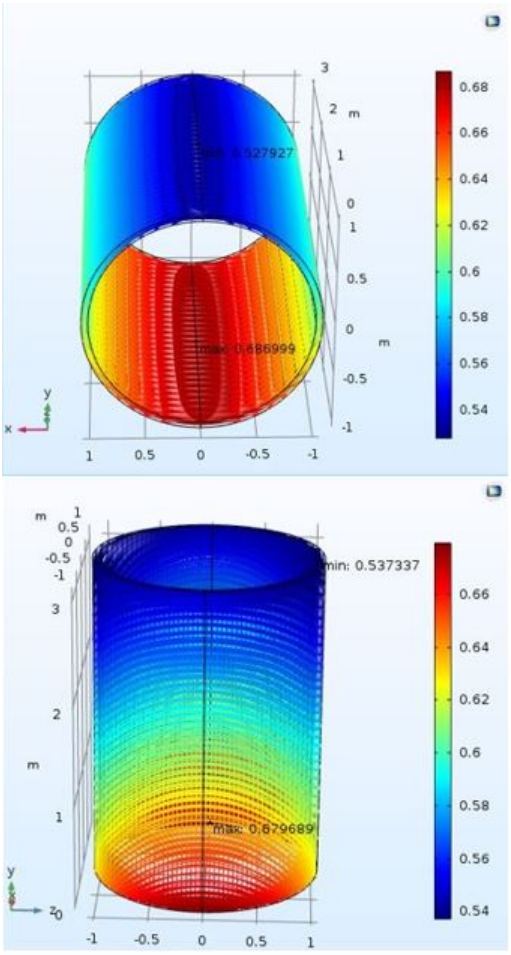

Fig. 8 Annular vertical and horizontal mass fraction fields in 3D porous cylindrical cells for $K_2 = 2.5 \times 10^{-11}$ m^2 and $R = 1.06$.

Table 4 Comparison of maximum and minimum mass fractions values in vertical annular cell between spectral method and Comsol Multiphysics for $R_i = 0.05$ m, 0.1 m, 0.2 m, 0.3 m for fixed $\delta T = 10°$C and for $K_2 = 2.5 \times 10^{-11}$ m^2.

R_i	Comsol		Spectral method	
	C_{max}	C_{min}	C_{max}	C_{min}
0.05	0.6475	0.5719	0.646	0.572
0.1	0.6804	0.5372	0.680	0.537
0.2	0.7498	0.4678	0.750	0.468
0.3	0.8191	0.3985	0.819	0.398

Table 5 Comparison of maximum and minimum mass fractions values in horizontal annular cell between spectral method and Comsol Multiphysics for $R_i = 0.05$ m, 0.1 m, 0.2 m, 0.3 m for fixed $\delta T = 10°$C and for $K_2 = 2.5 \times 10^{-11}$ m^2.

R_i	Comsol		Spectral method	
	C_{max}	C_{min}	C_{max}	C_{min}
0.05	0.6508	0.5652	0.651	0.565
0.1	0.6871	0.5273	0.687	0.527
0.2	0.7595	0.4517	0.759	0.452
0.3	0.8320	0.3762	0.832	0.376

Table 6 Maximum and minimum mass fractions in vertical and horizontal annular cells for $R_i = 0.1$ m, 0.2 m, and 0.3 m for fixed $\delta T = 10°$C and for $K_1 = 6.58 \times 10^{-10}$ m^2.

R_i	Vertical cell		Horizontal cell	
	C_{max}	C_{min}	C_{max}	C_{min}
0.1	0.6133	0.6043	0.6236	0.5982
0.2	0.6165	0.6010	0.6338	0.5898
0.3	0.6200	0.5980	0.6444	0.5813

Table 7 Maximum and minimum mass fractions in vertical and horizontal annular cells for $\delta T = 10, 15, 20, 25°$C for $R_i = 0.1$ m, $K_2 = 2.5 \times 10^{-11}$ m^2.

δT	Vertical cell		Horizontal cell	
	C_{max}	C_{min}	C_{max}	C_{min}
10	0.6804	0.5372	0.6871	0.5273
15	0.6900	0.5276	0.7134	0.5009
20	0.6945	0.5231	07328	0.4822
25	0.6971	0.5205	0.7483	0.4680

4.3 Verification of the hypothesis $C(1-C) = C_0(1-C_0)$

In order to verify the validity of the hypothesis introduced in the mathematical formulation of the problem, direct numerical simulations were performed when $C(1-C) \neq C_0(1-C_0)$. Table 8 and Table 9 show that the hypothesis can no longer be adopted for $R_i > 0.3$m because the difference between mass fraction values, for $C(1-C) \neq C_0(1-C_0)$, would be relatively important.

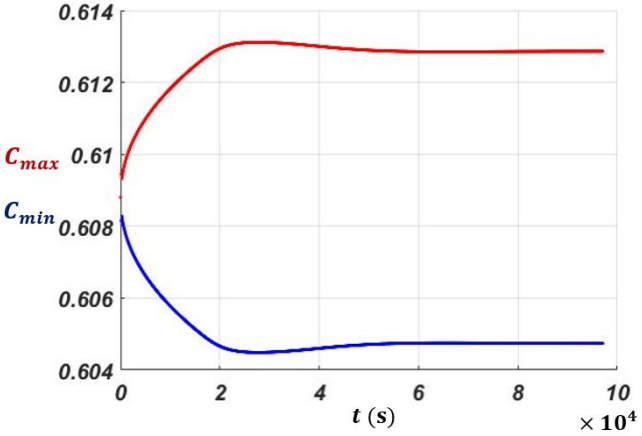

Fig. 9 Variation of C_{max} (in red) and C_{min} (in blue) as a function of time in vertical annular cell for: $R_i = 0.1$ m $e = 6 \times 10^{-3}$ m and $\delta T = 10°$C for $K_1 = 6.58 \times 10^{-10}$ m^2.

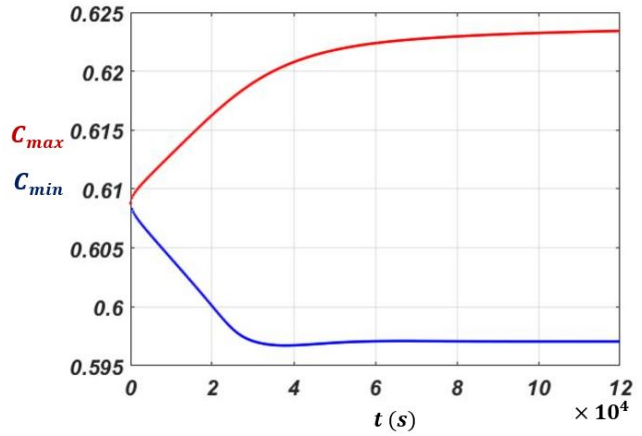

Fig. 10 Variation of C_{max} (in red) and C_{min} (in blue) as a function of time in horizontal annular cell for: $R_i = 0.1$ m $e = 6 \times 10^{-3}$ m and $\delta T = 10°$C for $K_1 = 6.58 \times 10^{-10}$ m^2.

For this reason, all the cases studies were limited to configurations where $R_i \leq 0.3$ m.

Table 8 Comparison of maximum and minimum mass fractions values in vertical annular cell between considering or not the hypothesis $C(1-C) = C_0(1-C_0)$ for $R_i = 0.05$ m, 0.1 m, 0.2 m, 0.3 m and 0.4 m for fixed $\delta T = 10°$C and for $K_2 = 2.5 \times 10^{-11}$ m^2.

R_i	$C(1-C) \neq C_0(1-C_0)$		$C(1-C) = C_0(1-C_0)$	
	C_{max}	C_{min}	C_{max}	C_{min}
0.05	0.6451	0.5713	0.6457	0.5719
0.1	0.6782	0.5359	0.6804	0.5372
0.2	0.7401	0.4654	0.7498	0.4678
0.3	0.7948	0.3977	0.8191	0.3985
0.4	0.8413	0.3349	0.8886	0.3290

Table 9 Comparison of maximum and minimum mass fractions values in horizontal annular cell between considering or not the hypothesis $C(1-C) = C_0(1-C_0)$ for $R_i = 0.05$ m, 0.1 m, 0.2 m, 0.3 m and 0.4 m for fixed $\delta T = 10°$C and for $K_2 = 2.5 \times 10^{-11}$ m^2.

R_i	$C(1-C) \neq C_0(1-C_0)$		$C(1-C) = C_0(1-C_0)$	
	C_{max}	C_{min}	C_{max}	C_{min}
0.05	0.6505	0.5649	0.6508	0.5652
0.1	0.6854	0.5267	0.6871	0.5273
0.2	0.7488	0.4497	0.7595	0.4517
0.3	0.8005	0.3713	0.8320	0.3762
0.4	0.8387	0.2921	0.9044	0.3006

4.4 Mass fraction fields and streamlines in the two configurations

In fig.11 and fig.12, the steady state mass fraction field and the streamlines in the horizontal annular cell and in the vertical annular cell are presented. It can be observed for the horizontal configuration that the velocity field is almost tangential except near the azimuth angles $\theta = 0$ or π. For the vertical configuration the velocity field is almost vertical except near the two extremities of the cell.

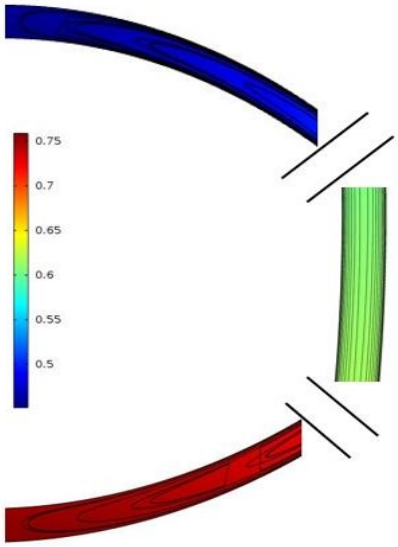

Fig. 11 Iso-C and streamlines in an annular horizontal cell*$R_i = 0.2$ m, $e = 6 \times 10^{-3}$ m and $\delta T = 10°$C and $K_2 = 2.5 \times 10^{-11}$ m^2.
*the scales are not respected in order to clearly visualize the mass fraction field and the streamlines.

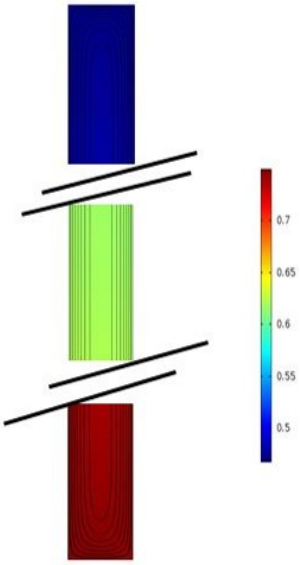

Fig. 12 Iso-C and streamlines in an annular vertical cell*$R_i = 0.2$ m, $e = 6 \times 10^{-3}$ m and $\delta T = 10°$C and $K_2 = 2.5 \times 10^{-11}$ m^2.
*the scales are not respected in order to clearly visualize the mass fraction field and the streamlines.

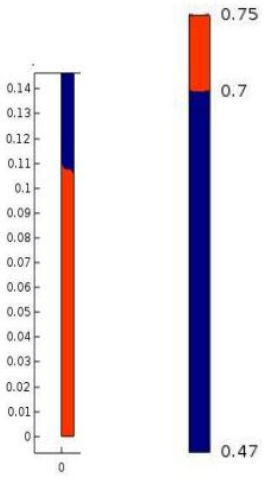

Fig. 13 Calculation of Vol_1.

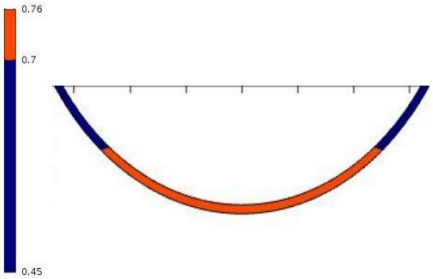

Fig. 14 Calculation of Vol_2

4.5 Amount of species separated at the bottom and the top of the two cells

The two previously mentioned configurations (fig.11 and 12) were considered. The difference between these two configurations is mainly due to the amount of species separated at the top or the bottom of the cells.The useful volume in the vertical cell where the denser component with $C > 0.7$ can be collected is obtained by: $Vol_1 = e(0.1075)\pi(R_i + R_o) = 8.2 \times 10^{-4}$ m^3 (cf. Fig.13).
In the horizontal annular cell, the volume where the denser component with $C > 0.7$ can be collected is approximately: $Vol_2 = (\pi\frac{(R_o^2 - R_i^2)}{4}\pi R_i) = 12 \times 10^{-4}$ m^3 (cf. Fig.14).
The amount of species separated at the bottom or top of the cells is about one and a half times bigger for the horizontal annular cell than for the vertical annular cell.

5 Conclusion

This paper focuses on the species separation in a vertical and in a horizontal porous cylindrical annular cell. The cells are filled with a porous medium saturated by a water-ethanol mixture (60.88% water). The thickness of the two cells is $e = R_o - R_i \ll R_i$ where R_i and R_o are respectively the inner and outer radius of the cylinder. For the vertical thermogravitational column, we succeeded in finding the analytical solution of the thermal, velocity and mass fraction fields. Two alternative solutions were obtained in the case where $e \ll Ri$. The first one (V_2) corresponds to the case where the annular geometry approaches the parallelipipedic thermogravitational column while the second one (V_3) takes into account the curvature of the annular geometry. A good agreement was observed between these two solutions. The governing equations and the associated boundary conditions were solved numerically using a finite element method with Comsol Multiphysics sofware. For $R_i = 0.005$, 0.1, 0.2 and 0.3 m, $e = 0.006$ m, $\delta T = 10°$C, $K_2 = 2.5 \times 10^{-11}$ m^2, the results were compared with those obtained by a spectral collocation

method with Gauss-Lobatto-Chebyshev points. The results obtained by these two methods were in good agreement. The influence of R_i and δT on the species separation were investigated as well as the permeability of the porous medium. For two cylindrical annular columns of the similar geometric dimensions, the amount of species separated from the same binary mixture is 1.5 higher in the horizontal column than in the vertical column. On the other hand the time necessary to reach the stationary state in the vertical column is almost twice as short as the one necessary to reach the stationary state in the horizontal column.

Acknowledgements This work was supported by CNES, the French National Space Agency.

References

1. D.A. Nield, A. Bejan, Convection in Porous Media (third ed.) Springer Verlag, New York, (2006).
2. K. Vafai, Handbook of Porous Media second editions, Taylor and Francis, New York, pp. 269-320 (2005).
3. J.C. Legros, Y. Gaponenko, A. Mialdun, T. Triller, A. Hammon, C. Bauer, W. Köhler, V. Shevtsova, Phys. Chem. Chem. Phys. **17**, 27713 (2015).
4. W. Köhler, K.I. Morozov, The Soret effect in liquid mixtures, J. Non-Equilibrium Thermodyn. **41**(3), 151–197 (2016).
5. W.H. Furry, R.C. Jones, L. Onsager, On the theory of isotope separation by thermal diffusion, Phys. Rev. **55**, 1083–1095 (1939).
6. M. Lorenz and A. H. Emery, The packed thermal diffusion column. Chem. Eng. Sci. **11**, 16- 23 (1959).
7. J.K. Platten, M.M. Bou-Ali, J.F. Dutrieux, Enhanced molecular separation in inclined thermogravitational columns, J. Phys. Chem. B, **107**(42), 11763–11767 (2003).
8. M. C. Charrier-Mojtabi, B. Elhajjar, A. Mojtabi, Analytical and numerical stability analysis of Soret driven in a horizontal porous layer, Physics of fluids, **19**, 124104 (2007).
9. B. Seta, A. Errarte, D. Dubert, J. Gavaldà, M.M. Bou-Ali, X. Ruiz, Gravitational stability analysis on double diffusion convection in ternary mixtures, Acta Astronautica **160**, 442-450 (2019).
10. B. Elhajjar, A. Mojtabi, M.C. Charrier-Mojtabi, Separation of a binary fluid mixture in a porous horizontal cavity, Physical Rev. E **77**(2), 026310 (2008).
11. B. Elhajjar, A. Mojtabi, P. Costesèque, M.C. Charrier-Mojtabi, Separation in an inclined porous thermogravitational cell, Int. J. of Heat and Mass transfer, **53**,I.21-22, 4844-4851 (2010).
12. A. Khouzam, A. Mojtabi, M.C. Charrier-Mojtabi, B. Ouattara, Species separation of a binary mixture in the presence of mixed convection, Int. J. Therm. Sci. **73**, 18-27 (2013).
13. L. Yacine, A. Mojtabi, R. Bennacer, A. Khouzam, Soret-driven convection and separation of binary mixtures in a horizontal porous cavity submitted to cross heat fluxes, Int. J. Therm. Sci. **104**, 29–38 (2016).
14. V. Yasnou, A. Mialdun, D. Melnikov, V. Shevtsova, Role of a layer of porous medium in the thermodiffusion dynamics of a liquid mixture, Int. J. of Heat and Mass transfer, **143**, 118480 (2019).
15. A. Mojtabi, A. Khouzam, Y. Loujaine, M.C. Charrier-Mojtabi, Analytical and numerical study of Soret mixed convection in two sided lid-driven horizontal cavity: Optimal species separation, Int. J. of Heat and Mass transfer, **139**, 1037-1046 (2019).
16. O. Abahri, D. Sadaoui, K. Mansouri, A. Mojtabi, M.C. Charrier-Mojtabi, Thermogravitational separation in horizontal annular porous cell. Mech Ind, **18**(106) (2017).
17. B. Seta, E. Lapeira, D. Dubert, F. Gavalda, M.M. Bou-Ali, X. Ruiz, Separation under thermogravitational effects in binary mixtures, Eur. Phys. J. E, **42**(58) (2019).
18. H. Nasrabadi, H. Hoteit, A. Firoozabadi, An analysis of species separation in a thermogravitational column filled with a porous medium, Transp Porous Med, **67**, 473–486 (2007).
19. A. Mojtabi, K. Sioud, A. Bergeon, M.C. Charrier-Mojtabi, Numerical and Analytical Studies of Soret-Driven Convection Flow Inside an Annular Horizontal Porous Cavity, Fluids, **6**, 357 (2021).
20. A. Mojtabi and J.P. Caltagirone, Energy stability of a natural convective flow in a horizontal annular space, Physics of Fluids, **67**(6), (1979).

Appendix A: Expression of m_2, $h_2(r)$, m_3 and $h_3(r)$

$$m_2 = -108Le(R-1)A(-ln(R)^2R + (R-1)^2)R_{aT}^2 /(54R^2ln(R)^3Le^2R_{aT}^2 - (9(-12 + (Le^2R_{aT}^2 - 12)R^2 + (3Le^2R_{aT}^2 + 24)R))(R-1)ln(R)^2 + 3Le^2RR_{aT}^2 (R-17)(R-1)^2ln(R) + R_{aT}^2Le^2(R^2+R+28)(R-1)^3)$$

$$h_2(r) = C_0 + \frac{1}{36(R-1)^2ln(R)}(18Leln(R)^2R^2R_{aT}m_2 - (36(R-1))((1/2)Le\ln(r)RR_{aT}m_2 + R((1/12)LeRm_2 + Le(-(1/4)r^2 + 5/6)m_2 + A)R_{aT} + (1/2)Hm_2 (R-1))ln(R) + (36((Le(1/4 - (1/4)r^2)m_2 + A)ln(r) - (1/36)R^2m_2Le - (1/36)LeRm + 2m_2Le(1/9) + A)) (R-1)^2R_{aT})$$

$$m_3 = -(16ALeR_{aT}^2(R^6 - 4\ln(R)^2R^4 + 4\ln(R)^2R^2 - 3R^4 + 3R^2 - 1))/(32R^4\ln(R)^3Le^2R_{aT}^2 + 64(R-1)^3 (R+1)^3\ln(R)^2 - 12Le^2R^2R_{aT}^2(R-1)^2(R+1)^2\ln(R) + Le^2R_{aT}^2(R^2+1)(R-1)^3(R+1)^3)$$

$$h_3(r) = C_0 + \frac{1}{32(R^2-1)^2\ln(R)}(16Le\ln(R)^2R^4R_{aT}m_3 - 32(\frac{\ln(r)R^2m_3LeR_{aT}}{2} + (Le(\frac{3}{8} - \frac{r^2}{4})m_3 + A)R^2R_{aT} + \frac{Hm_3(R-1)(R+1)}{2})(R-1)(R+1)\ln(R) + 32((-\frac{Lem_3r^2}{4} + A)\ln(r) - \frac{3R^2m_3Le}{32} + Le(\frac{r^2}{8} - \frac{3}{32})m_3 + \frac{A}{2})R_{aT} (R-1)^2(R+1)^2)$$